Chemically Fabricated Magnetic Quantum Dots of InP:Mn

Y. Sahoo,[†] P. Poddar,[‡] H. Srikanth,[‡] D. W. Lucey,[†] and P. N. Prasad*[,†]

Institute for Lasers, Photonics and Biophotonics, The State University of New York at Buffalo, Buffalo, New York 14260, and Materials Physics Laboratory, Department of Physics, University of South Florida, Tampa, Florida 33620

Received: January 11, 2005; In Final Form: May 23, 2005

Quantum dots of InP:Mn are chemically prepared by following hot colloidal nanochemistry with starting precursors that obviate the need for external surfactant. These quantum dots are uniform spheres with 3-nm diameters; they are crystalline, photoluminescent, and magnetic. The crystallographic and optical properties are similar to those of undoped InP nanocrystallites, while the magnetism is consistent with the ferromagnetic response observed in a class of diluted magnetic semiconductors. Because of the ultrafine sizes, the sample shows superparamagnetic behavior, whereas ferromagnetic hysteresis loops are clearly seen below the blocking temperature. Structural characterization and analysis confirm that the magnetism in these quantum dots is not due to segregated binary MnP or MnO phases and that they truly represent a homogeneous dilute magnetic semiconductor.

Introduction

Semiconductor nanocrystallites with sizes less than their bulk Bohr radii have now been universally recognized as an important class of materials due to changes in their properties associated with quantum size effects.[1−3] The challenge of precisely correlating their properties, in a systematic fashion, to their sizes has been addressed successfully due to advanced preparation methods that have rendered control over the sizes and shapes of these nanoparticles. Impurity doping in quantum-confined nanocrystals provides an opportunity for manipulating carrier density or introducing an impurity Coulomb field that can affect the dynamics of electron−hole pairs and influence magnetooptic properties.[4] Successful doping of magnetic impurities in semiconductor quantum dots (QDs) yields a new paradigm as a zero-dimensional counterpart of the well developed diluted magnetic semiconductor (DMS) bulk and thin film systems, which could potentially lead to the fabrication of novel magnetooptic and magnetoelectronic devices.[5−7] It has been widely acknowledged that while impurity doping in bulk semiconductors is now routine, the extension to semiconductor nanocrystals is very difficult to achieve.[4,8] For example, while a heavily doped bulk semiconductor typically has about 1 dopant for every 10^5 atoms, a colloidal QD with a 5-nm size (roughly 1000 atoms) does not have room for even one impurity atom unless the impurity concentration is enhanced by 2 orders of magnitude. Therefore, new methodologies with systematic parametric controls are called for to develop doped quantum dots with impurity atoms well entrenched within the lattice. Mn doped II−VI quantum dots have been reported by a moderate number of past studies where a chemical route has been used.[9−11] The literature reports on Mn doped III−V systems are relatively few, probably because of the more involved preparation methods typically required in III−V semiconductor quantum dots. Korgel's team has reported up to 5% Mn doped InAs quantum dots by a chemical route where the sample remains paramagnetic down to the temperature 5 K.[8] In a very recent work, Brock and coworkers[12] have prepared Mn doped InP by a coordinating solvent colloidal route and detected paramagnetic Curie−Weiss behavior. In this paper, we report fabrication of Mn doped InP nanocrystals prepared in a noncoordinating solvent from a custom-made indium precursor. The sample shows ferromagnetic characteristics at low temperature, a significant finding in DMS QDs.

Experimental Section

Synthesis. The Mn doped InP particles were made by the widely recognized hot colloidal synthetic route. In our laboratory, we developed a method of preparing semiconductor quantum dots that obviates the need for any external surfactant.[13,14] The preparation was carried out by reacting indium myristate (prepared as per ref 14), manganese acetylacetonate, and tristrimethylsilylphosphine in octadecene. In a typical reaction, 0.1594 g of indium myristate and 0.0140 g of manganese acetylacetonate (20% molar ratio with indium myristate) were dissolved in 20 mL of dry octadecene at 300 °C under argon. Subsequently, 0.0321 g of tristrimethylsilylphosphine in 2 mL of dry octadecene was injected into the reaction flask. The reaction temperature was immediately forcedropped by adding 20 mL more of dry octadecene kept at room temperature and the reaction was made to continue for a total of 3 h, allowing the growth and annealing of the resulting nanoparticles. At the end of the reaction, the sample was collected from the reaction flask, 25 mL each of acetone and ethanol were added, and the mixture was centrifuged. After the supernatant was decanted out, 50 mL of ethanol was added to the precipitate and the resulting mixture was sonicated for 10 min, followed by another round of centrifugation. The cycle of ethanol washing and sonication was repeated twice. After the final wash, most of the sample was collected as a dry powder and some portion was kept as a solution in hexane for optical studies. The product was characterized by transmission electron microscopy (TEM), energy dispersive X-ray spectroscopy (EDS), X-ray photoelectron spectroscopy (XPS), X-ray diffrac-

* Corresponding author. E-mail: pnprasad@buffalo.edu.
[†] The State University of New York at Buffalo.
[‡] University of South Florida.

10.1021/jp050202n CCC: $30.25
Published on Web 07/22/2005

tion (XRD), photoluminescence (PL), photoluminescence excitation (PLE), and magnetometry.

Transmission Electron Microscopy (TEM). TEM images were acquired using a JEOL 100 CX II microscope operating at an acceleration voltage of 80 kV in the bright field mode.

Energy Dispersive X-ray Spectroscopy (EDS). EDS was obtained with a Hitachi S-4000 field emission scanning electron microscope. The microscope operates at an electron acceleration voltage of 20 kV. The powder sample was cast on a silicon or graphite substrate. The X-ray fluorescence beams were collected with an X-ray collection unit IXRF 500 system.

X-ray Photoelectron Spectroscopy (XPS). XPS studies were performed on a Physical Electronics/PHI 5300 X-ray photoelectron spectrometer with a hemispherical analyzer and a single channel detector, operated at 300 W (15 kV and 20 mA). Mg Kα radiation (1253.6 eV) and pass energies of 89.45 eV for survey scans and 17.9 eV for high-resolution scans were used.

X-ray Diffraction (XRD). X-ray diffraction was taken on a Siemens X-ray diffractometer model D500 with a Cu Kα source. A powder of the sample was placed on a glass slide, and scanning angles were slowly varied by rotating the sample geometry. The 2θ angles probed were from 3° to 60°, scanned at a rate of 2° per minute.

Photoluminescence (PL) and Photoluminescence Excitation (PLE). PL and PLE spectra were acquired in the frontal geometry using a Jobin Yvon Fluorolog-3 spectrofluorometer, equipped with a 400 W Xe lamp as an excitation source and a Hamamatsu R928 photomultiplier (PMT) tube as a detector.

Electron Paramagnetic Resonance (EPR). The EPR spectra were obtained on Bruker Data System ESP 3220 equipment at an applied microwave frequency of 9.75 GHz and a modulating frequency of 100 kHz. About 40 mg of powder sample was placed in an EPR tube, and EPR was measured at both room temperature and low temperature (103 K).

Magnetization. Direct current (dc) magnetization measurements were performed using a Physical Property Measurement System (PPMS) from Quantum Design, equipped with a 7 T superconducting magnet. Zero-field-cooled (ZFC) and field-cooled (FC) measurements were done at 100 Oe magnetic fields. Low-temperature magnetization data were acquired from a lowest temperature of 2 K.

Results and Discussion

The reaction between indium carboxylate (myristate or laurate) and tristrimethylsilylphosphine without the need for external surfactant has been established to yield monodispersed InP nanoparticles with a temporal evolution of sizes.[14] The same reaction in the presence of the manganese precursor, manganese acetylacetonate, is found to successfully incorporate the Mn ion as a dopant. The TEM image (Figure 1) shows that the particles are uniform, sized at a median value of ~3 nm, and spherical in shape.

The X-ray diffractogram (Figure 2) shows the $\langle 111 \rangle$, $\langle 220 \rangle$, and $\langle 311 \rangle$ planes at the 2θ values 26.3°, 44°, and 51.9°, respectively, which closely agrees with the bulk zinc blende structure and is also consistent with the bulk lattice parameter 5.87 Å.[15] There is no evidence of a change in the lattice constant due to Mn doping. An extra peak at the 2θ value 21.40° originates from the unreacted indium myristate. A small percentage of indium myristate is usually detected despite several washes in ethanol. We critically examined the results and confirmed that there was no indication of MnP phases. MnP crystallographically occurs as the B31 orthorhombic phase with the lattice parameters $a = 5.917$ Å, $b = 5.260$ Å, and $c = 3.173$ Å, and the dominant peaks are $\langle 211 \rangle$ and $\langle 121 \rangle$ at a 2θ value ~ 48°, at which the diffractogram of our sample shows no peaks.[16] The average domain size of these quantum dots is extracted from the full width at half-maximum (fwhm) of the most intense peak by applying the Scherrer formula

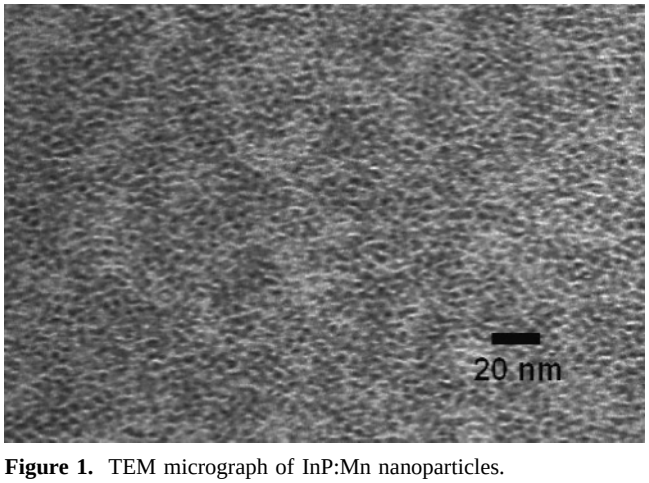

Figure 1. TEM micrograph of InP:Mn nanoparticles.

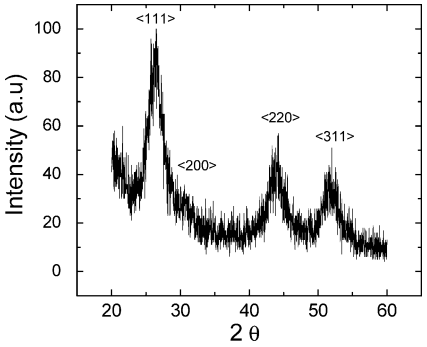

Figure 2. X-ray diffraction pattern of InP:Mn.

$$d = \frac{0.9\lambda}{B \cos \theta}$$

where d is the average crystallite size, λ the wavelength of the X-ray, B the fwhm in units of radians, and θ the diffraction angle in degrees.

It is common practice to obtain the domain sizes from lower angle diffraction peaks, as stacking faults and polytypism make the calculation less reliable at higher angles.[10,18] From the $\langle 111 \rangle$ peak, the crystalline domain size is calculated to be ~2.6 nm, which is in fair agreement with the TEM result. The composition of the particles, as analyzed with XPS and EDS, confirms the presence of Mn.

In Figure 3a, showing the high-resolution XPS spectrograph of In and P, we notice the well separated characteristic peaks of the In $3d_{5/2}$ and $3d_{3/2}$ electrons as well as the peaks of the P 3p core level electrons from InP (130 eV) and oxidized phosphorus (~133 eV).[15] The intensity of the latter peak is quite significant, because of the increase in oxidized phosphorus species caused by multiple washings of the precipitate in acetone or ethanol, adapted from our work on InP.[14] As shown in Figure 3b, there is a peak at ~644 eV, attributable to Mn species, and an intense peak at ~670 eV, resulting from the overlap of a Mn Auger effect and In $3p_{3/2}$. The former peak may not arise from any of the manganese oxides such as MnO, MnO_2, Mn_3O_4, and Mn_2O_3, all of which appear in the range 641−642 eV,[19] or from MnP, which occurs at 639 eV.[17] It is difficult to judge the accurate oxidation state of Mn or its exact chemical environment

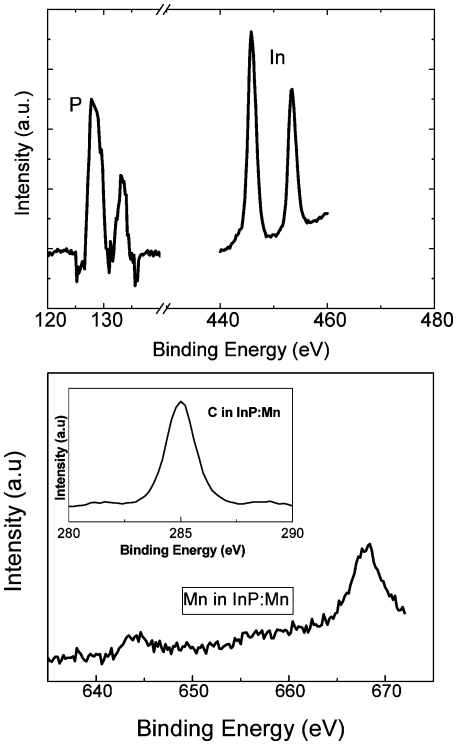

Figure 3. (a) High-resolution XPS of InP:Mn quantum dots showing In $3d_{5/2}$ and $3d_{3/2}$ and P 3p core levels. (b) High-resolution XPS of InP:Mn quantum dots showing C and Mn peaks.

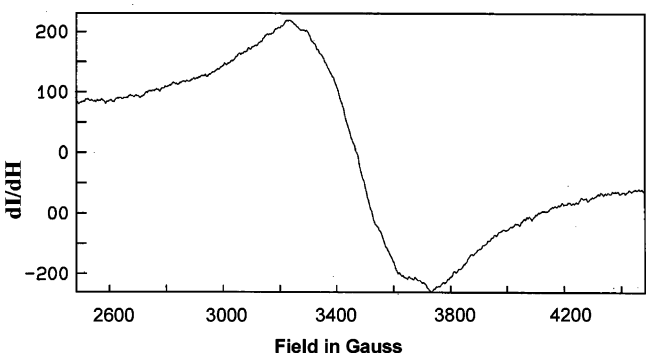

Figure 4. Room-temperature EPR spectrum of InP:Mn.

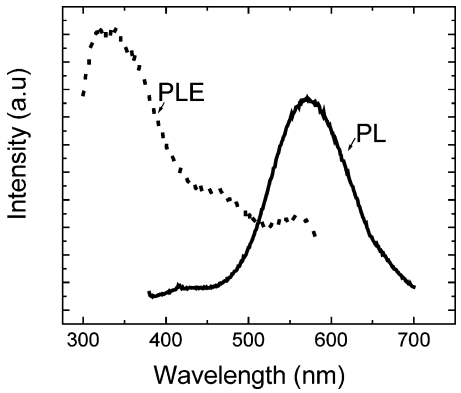

Figure 5. PL and PLE of InP:Mn nanoparticles in hexane dispersion.

in our sample, since the binding energy seems to be higher than those for most of the Mn species reported in the literature. It should be noted here that all the spectra discussed above are calibrated by the carbon peak that occurs at 285 eV. Therefore, the spectra are devoid of any zero-shift error. As is well-known, the sampling depth of XPS is rather low (a few angstroms to a few tens of angstroms, depending on the grazing angle of the X-ray). Therefore, in the event of an abundance of surfactant (in our case, in situ generated surfactant) on the surface despite multiple washings, the actual concentrations of the constituent atoms, i.e., In, P, and Mn, are overwhelmed by the percentages of carbon and oxygen. For the actual concentrations, EDS data can be treated relatively more dependably because the sampling depth is higher (~100 nm to 1 μm). We estimate that In:P:Mn ratios are 1.0:0.57:0.09 and 1.0:0.45:0.12 from the XPS and EDS, respectively. The percentage of In is higher than that of P because of the small quantity of inseparable indium myristate, which we estimated to be less than 10%, and also because indium atoms preferentially populate the surface of the nanoparticles. Therefore, we are only using the XPS and EDS data to exclusively assign the percentage of Mn dopant concentrations. Thus, on the basis of the proportion of Mn found from XPS (9%) and EDS (12%), we assign the percentage of Mn in our sample InP:Mn at ~10%.

The EPR measured at room temperature as well as at 103 K shows the peak pertaining to the presence of Mn in the sample, with the first derivative peak centered at 3470 G (Figure 4). To describe the behavior of the Mn ion in a host lattice environment, it is helpful to recall the spin Hamiltonian[20,21]

$$H = g\beta\vec{H}\cdot\vec{S} + ASI + {}^1/_6 a(S_x^4 + S_y^4 + S_z^4) + D\{S_z^2 - {}^1/_3 S(S+1)\}$$

where g is the gyromagnetic ratio, β is the Bohr magneton, H is the applied magnetic field, and A and D are the EPR parameters. The first term represents the Zeeman interaction; the second term, the hyperfine interaction of an unpaired electron (d^5 system) with the ^{55}Mn nucleus; the third term, the cubic field splitting; and the fourth term, the fine structure splitting, which is absent in a cubic environment. Here, it should be noted that the hyperfine splitting (electronic−nuclear interaction) should manifest producing a fine structure sextet in the EPR peak, when the Mn^{2+} ion is resident in a cubic field. In our sample, the hyperfine splitting does not have a pronounced presence at room temperature or even at low temperature (not shown). However, it still does not mean that Mn^{2+} stays in a noncubic lattice environment, for there are other factors that govern this behavior, as explained below. There are past studies of Mn doped quantum dots where hyperfine splitting depended on the concentration of the dopant. Sapra et al.,[10] Borse et al.[21] (for Mn doped ZnS), and Stowell et al.[8] (for Mn doped InAs nanocrystals) have noted that the sextet structure weakens as the concentration of Mn in the sample increases. Wash out of the sextet structure has been primarily attributed to Mn−Mn interaction. We believe that the Mn concentration (approximately 10% from the XPS and EDS) in our sample is too high a dopant concentration level where the hyperfine splitting may be expected.

The PL shows (Figure 5) a spectrum with a maximum at 570 nm and a fwhm at 110 nm. Akin to literature reports, e.g., concerning Mn doped ZnS, it is possible that, besides band edge excitonic recombination within the InP quantum dots, a nonradiative decay from the conduction band to the Mn^{2+} d level takes place followed by a radiative intraband transition. The intraband $^4T_1 - {}^6A_1$ transition (within the 3d orbitals) of Mn is expected to give rise to an orange emission,[10] which, in our study, could easily be enveloped by the original PL profile of the InP quantum dots. PLE shows three broad maxima, peaking at 337, 470, and 560 nm, which are very similar to that of the undoped dots produced by the same method.[14] It is, therefore, not possible to estimate the contribution of Mn^{2+} dopant to the

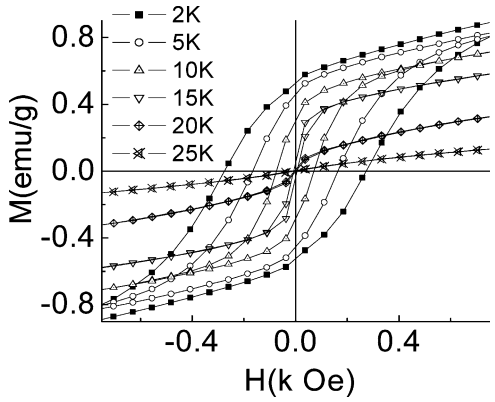

Figure 6. Magnetization vs magnetic field curves for InP:Mn quantum dot powder.

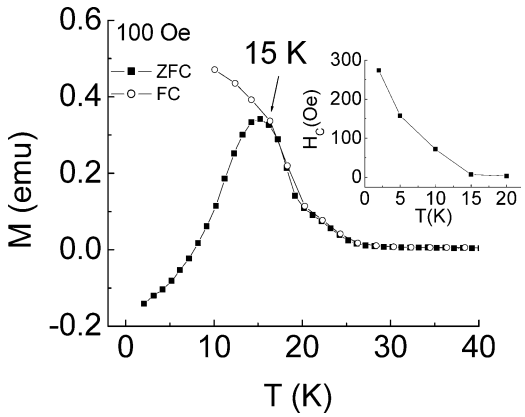

Figure 7. ZFC and FC magnetization curves. The inset shows the temperature dependence of coercivity.

overall PL property of this system. A detailed lifetime measurement could help resolve this question.

The magnetization vs magnetic field curves of the sample have been plotted in Figure 6 at different temperatures. It is evident from these curves that at 25 K the sample behaves like a paramagnet, where the magnetization shows a linear dependence on field. The ferromagnetic ordering sets in below 25 K as the magnetization curves start exhibiting nonlinearity. Down to 15 K, the InP:Mn quantum dots show purely superparamagnetic behavior with reversible nonlinear magnetization with zero or very small coercivity (7 Oe at 15 K). The magnetization of the sample did not saturate even at the highest field of 2.5 T. This behavior is reminiscent of a spin glass like transition not uncommon in ultrafine magnetic particles.[22]

Below 15 K, distinct hysteretic response sets in and the loop starts broadening with a coercivity of 72 Oe at 10 K and 274 Oe at 2 K. This irreversible behavior is consistent with the expected response for a collection of frozen single-domain spins below the blocking temperature.

The coercive fields plotted against temperature (inset of Figure 7) scale according to the relationship

$$H_c \sim T^{0.5}$$

at the lower end of the temperature scale (from 2 to 15 K approximately). This law is exhibited by an ensemble of noninteracting superparamagnetic particles.[23,24] Of course, there are many reports where superparamagnetic particles show departure from this behavior due to strong interaction, dipolar or otherwise.[25,26] From the observed behavior, we believe that our sample consists of weakly interacting particles.

The ZFC and the FC magnetization curves were measured at low temperatures with an applied field of 100 Oe. The curves overlap at high temperatures with a narrow cusp in the ZFC at ~15 K where they start diverging from each other as the temperature is lowered further. This is also consistent with the blocked state of the superparamagnetic moments below this temperature and agrees well with the emergence of coercivity in the magnetization curves below 20 K. A Curie−Weiss fit was attempted on the ZFC curve above the blocking temperature. Taking into account about 20% mass contribution by the associated surfactant monolayer on a 3-nm particle surface, magnetic moments per gram of the sample were estimated to be $\sim 2.068 \times 10^{20}$ Bohr magnetons (β), which translated to 18.2 β per particle.[33] This is equivalent to only three high-spin Mn^{2+} atoms per particle if one assigns an average of ~5.9 β per Mn atom, estimated for a differently prepared InP:Mn particle system by Somaskandan et al.[12] Significantly lower values up to 2.2 β per Mn atom have been detected for InAs systems, as discussed in the report by Stowell et al.[8] Yet, at a 10% dopant concentration of Mn, which is equivalent to 28 Mn atoms per particle, the observed magnetic moment is very low. We note, however, that the estimate would contain errors associated with multiple sources such as uncertainty in the actual fraction of surfactant and also the Curie−Weiss fit being tried only in a small range of temperatures. There are instances in DMS systems where Mn spins exhibit canting and antiferromagnetic coupling that produce a partially disordered spin glass like magnetic state, thus, reducing the effective magnetic moment.[27] We believe that such a spin glass like ordering might actually occur in our DMS system, as also indicated by a nonsaturating magnetization even at high dc field (~20 kOe, not presented here). It may also be emphasized here that a corroborative value for magnetic moment per particle cannot be obtained from the saturation magnetization data because of the nonsaturating behavior of dc magnetization even at relatively high applied fields. The alternating current (ac) susceptibility measurements performed (step size of 0.3 K) in a frequency range from 10 Hz to 10 kHz also show a similar trend with considerable frequency dependence in the blocked state, supporting a spin glass like behavior (to be presented in detail in a separate article).

The appearance of ferromagnetism in DMS systems, particularly in $III_{1-x}MnV_x$, is usually explained in the framework of the Ruderman−Kittel−Kasuya−Yosida (RKKY) interaction or the carrier-induced ferromagnetism scenario, where the wave functions of the magnetic impurities and conduction band couple, as discussed by Ohno.[5] Because of the oscillatory nature of the RKKY interaction, both ferromagnetic and antiferromagnetic states can coexist in a random alloy type DMS. Within the mean-field approximation, the Curie temperature is determined by a competition between the ferromagnetic and antiferromagnetic interactions ($T_C = T_F - T_{AF}$), as studied by Dietl et al.[28] On the basis of the Zener model, they made a mean-field theoretical prediction for the Curie temperature in a DMS

$$T_C \propto J_{pd}{}^2 N_{Mn} \chi_h{}^P$$

where $\chi_h{}^P$ is the Pauli susceptibility of the hole system and N_{Mn} the number density of magnetic ions. Since J_{pd}, the exchange integral, is only weakly material dependent, the T_C will rise for larger concentrations of the magnetic Mn^{2+} and larger hole densities of states. On the basis of the modified Zener model, they calculated an ordering temperature of ~70 K for a 5% concentration of Mn and a high hole concentration of 3.5×10^{20} cm^{-3}. Though the model, as such, pertains to bulk DMS systems and may not effectively describe a QD DMS system

where surface disorder can possibly affect the J_{pd}, the exchange integral, higher Mn concentration is likely to enhance the probability of ferromagnetic ordering. Therefore, if a proper parametric control over a chemical reaction is established that entails control over the number of Mn ions and their ordering within the quantum dots, then a great deal of control over the magnetic properties can be attained. We believe that effects related to small size (~3 nm in the present case) might also have contributed to lowering the ordering temperature in our material in comparison to the theoretically expected value for 10% Mn doped InP. A theoretical as well as an experimental study on the effects of size variation from bulk to a few nanometers can shed some light to resolve this issue. There has been a great body of work on the maximization of Mn^{2+} concentration without making an irreversible crystallographic phase segregation. One such example is molecular beam epitaxial growth of digital alloys of (GaMn)As, so-called because of the distinct layers of Mn atoms sandwiched between the GaAs layers.[29] Exploring chemical precursors and optimizing chemical reactions that effectively dope Mn^{2+} in larger concentrations will be a significant step toward developing ferromagnetic semiconductor quantum dots on a large scale.

In the present work, the following factor needs to be considered with great attention. Any deleterious possibility of MnP phases in the sample that could give a misleading impression of ferromagnetism is ruled out from the following analyses. (1) In the bulk phase, MnP is a metallic compound exhibiting ferromagnetic order below $T_c \sim 291.5$ K and a screw-antiferromagnetic order (helimagnetic) below the Neel temperature, 47 K.[30] At nanoscale dimensions (sized 5.1 and 6.7 nm), MnP exhibits ferromagnetic ordering around the same temperature as its bulk counterpart, showing a nonlinear $M-H$ curve and superparamagnetic type behavior just below room temperature.[31] In our sample, we notice ferromagnetic ordering in the vicinity of 25 K and lower. (2) The XPS and EDS results suggest the presence of about 10% Mn atoms, an appreciable percentage. If these atoms were to give rise to the binary MnP, then an X-ray diffractogram would detect the extinctions due to the orthorhombic phase of the latter. On the basis of these observations, we are confident that the present system is composed of a truly doped DMS InP:Mn and rules out the presence of the MnP phase. At the end, it is worth glancing over the physics of MnO, a meek possibility in our sample. According to a recent study by Lee et al., MnO, which is an antiferromagnet in bulk, shows ferromagnetic ordering in nanosize at low temperature with an unusually high coercivity of ~9500 Oe at 2 K.[32] The origin of this huge coercivity in MnO nanocrystals is not yet explained. On the grounds of observed coercivity and structural characterization by XRD, the existence of MnO is ruled out.

In conclusion, we have synthesized InP:Mn quantum dots by hot colloidal nanochemistry with precursors not requiring any external surfactant. The products are magnetic quantum dots that show typical superparamagnetic and blocked ferromagnetic behavior at low temperatures. This finding is a step forward in the advancement of quantum dot spintronic materials, a field holding huge potential for novel magnetoelectronics and magnetooptics.

Acknowledgment. We thank Dr. Peter Bush for his help with the EDS experiment. The work at the State University of New York at Buffalo (UB) was supported by DURINT Grant No. F496200110358 from the Chemistry and Life Sciences Division of the Air Force Office of Scientific Research. The work at the University of South Florida (USF) was supported through DARPA/ARO Grant No. DAAD 19-03-1-0277.

References and Notes

(1) Prasad, P. N. *Nanophotonics*; John Wiley & Sons: New York, 2004.
(2) Alivisatos, A. P. *J. Phys. Chem.* **1996**, *100*, 13226.
(3) Murray, C. B.; Sun, S.; Gaschler, W.; Doyle, H.; Betley, T. A.; Kagan, C. R. *IBM J. Res. Dev.* **2001,** *45*, 47.
(4) Shim, M.; Wang, C.; Norris, D. J.; Guyot-Sionnest, P. *MRS Bull.* **2001**, *26*, 1005.
(5) Ohno, H. *Science* **1998**, *281*, 951.
(6) Bryan, D. J.; Gamelin, D. R. In *Progress in Inorganic Chemistry*; Karlin, K. D., Ed.; John Wiley & Sons: New York, 2005; Vol. 54, p 47.
(7) Furdyna, J. K.; et al. *Proceedings of NATO workshop on the optical properties of semiconductor quantum Nanostructures*; Sadowski, M. L., Potemski, M., Grynberg, M., Eds.; Kluwer Academic Publishers: Norwell, MA, 2000; p 211.
(8) Stowell, C. A.; Wiacek, R. J.; Saunders, A. E.; Korgel, B. A. *Nano Lett.* **2003**, *3*, 1441.
(9) Mikulec, F. V.; Kuno, M.; Bennati, M.; Hall, D. A.; Griffin, R. G.; Bawendi, M. G. *J. Am. Chem. Soc.* **2000**, *122*, 2532.
(10) Sapra, S.; Nanda, J.; Anand, A.; Bhat, S. V.; Sarma, D. D. *J. Nanosci. Nanotechnol.* **2003**, *3*, 1.
(11) Hanif, K. M.; Meulenberg, R. W.; Strouse, G. F. *J. Am. Chem. Soc.* **2002**, *124*, 11495.
(12) Somaskandan, K.; Tsoi, G. M.; Lowell, E. W.; Brock, S. L. *Chem. Mater.* **2005**, *17*, 1190.
(13) Furis, M.; MacRae, D. J.; Lucey, D. W.; Sahoo, Y.; Cartwright, A. N.; Prasad, P. N. *Mater. Res. Soc. Symp. Proc.* **2004**, *789*, 89.
(14) Lucey, D. W.; MacRae, D. J.; Furis, M.; Sahoo, Y.; Cartwright, A. N.; Prasad, P. N. *Chem. Mater.* **2005**, *17*, 3754.
(15) Guzelian, A. A.; Katari, J. E. B.; Kadavanich, A. V.; Banin, U.; Hamad, K.; Juban, E. Alivisatos, A. P.; Wolters, R. H.; Arnold, C. C.; Heath, J. R. *J. Phys. Chem.* **1996**, *100*, 7212.
(16) Huber, E. E., Jr.; Ridgley, D. H. *Phys. Rev. B* **1964**, *135*, A1033.
(17) Myers, C. E.; Franzen, H. F.; Anderegg, J. W. *Inorg. Chem.* **1985**, *24*, 1822.
(18) Bawendi, M. G.; Kortan, A. R.; Steigerwald, M. L.; Brus, L. E. *J. Chem. Phys.* **1989**, *91*, 7282.
(19) Wagner, C. D.; Riggs, R. M.; Davis, L. E.; Moulder, J. F. In *Handbook of Electron Spectroscopy*; Muilenberg, G. E., Ed.; Perkin-Elmer Corp., Physical Electronics: Eden Prairie, MN, 1979.
(20) Bershorn, M.; Baird, J. C. *An Introduction to Electron Paramagnetic Resonance*; W. A. Benjamin, Inc.: New York, 1966.
(21) Borse, P. H.; Srinvas, D.; Shinde, R. F.; Date, S. K.; Vogel, W.; Kulkarni, S. K. *Phys. Rev. B* **1999**, *60*, 8659.
(22) Bodker, F.; Morup, S.; Linderoth, S. *Phys. Rev. Lett.* **1994**, *72*, 282.
(23) Bean, C. P.; Livingstone, J. D. *J. Appl. Phys.* **1959**, *30*, 120S.
(24) Fonseca, F. C.; Goya, G. F.; Jardim, R. F.; Muccillo, R.; Carreno, N. L. V.; Longo, E.; Leite, E. R. *Phys. Rev. B* **2002**, *66*, 104406.
(25) McHenry, M. E.; Majetich, S. A.; Kirkpatrick, E. M. *Mater. Sci. Eng., A* **1995**, *204*, 19.
(26) Brunsman, E. M.; Scott, J. H.; Majetich, S. A.; McHenry, M. E.; Huang, M. Q. *J. Appl. Phys.* **1996**, *79*, 5293.
(27) Korzhavyi, P. A.; Abrikosov, I. A.; Smirnova, E. A.; Bergqvist, L.; Mohn, P.; Mathieu, R.; Svedlindh, P.; Sadowski, J.; Isaev, E. I.; Vekilov, Yu. Kh.; Eriksson, O. *Phys. Rev. Lett.* **2002**, *88*, 187202.
(28) Dietl, T.; Ohno, H.; Matsukura, F.; Cibert, J.; Ferrand, D. *Science* **2000**, *287*, 1019.
(29) Luo, H.; McCombe, B. D.; Na, M. H.; Mooney, K.; Lehmann, F.; Chen, X.; Cheon, M.; Wang, S.; Sasaki, Y.; Liu, X.; Furdyna, J. K. *Physica B* **2002**, *12*, 366.
(30) Ishikawa, Y.; Komatsubura, T.; Hirahara, E. *Phys. Rev. Lett.* **1969**, *23*, 523.
(31) Perera, S. C.; Tsoi, G.; Wenger, L. E.; Brock, S. L. *J. Am. Chem. Soc.* **2003**, *125*, 13960.
(32) Lee, G. H.; Huh, S. H.; Jeong, J. W.; Choi, B. J.; Kim, S. H.; Ri, H. C *J. Am. Chem. Soc.* **2002**, *124*, 12094.
(33) Assuming that the bulk density of InP (4.79 g cm^{-3}) is maintained for the InP:Mn particles, the mass of a 3-nm particle is 6.77×10^{-20} g. Therefore, each particle would have approximately 279 InP molecules. From the EDS and XPS data that suggest 10% atomic substitution, the Mn doping amounts to ~28 Mn atoms per particle. The Curie−Weiss fit gives the total net magnetic moment as 1.9184 g^{-1} after taking into account the 20% weight of surfactant that translates to 2.068×10^{20} β g^{-1}. Therefore, knowing that there are $(6.77 \times 10^{-20})^{-1}$ particles per gram, the magnetic moment per particle is estimated to be 18.2 β.